Article

# Mechanistic Insights into the Rhodium-Catalyzed Intramolecular Ketone Hydroacylation

Zengming Shen, Peter K. Dornan, Hasan A. Khan, Tom K. Woo, and Vy M. Dong

*J. Am. Chem. Soc.*, **2009**, 131 (3), 1077-1091 • DOI: 10.1021/ja806758m • Publication Date (Web): 07 January 2009



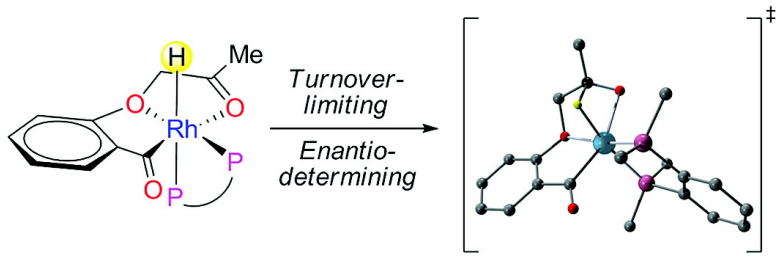


## More About This Article

Additional resources and features associated with this article are available within the HTML version:

- Supporting Information
- Access to high resolution figures
- Links to articles and content related to this article
- Copyright permission to reproduce figures and/or text from this article

View the Full Text HTML

J|A|C|S ARTICLES

Published on Web 01/07/2009

# Mechanistic Insights into the Rhodium-Catalyzed Intramolecular Ketone Hydroacylation

Zengming Shen,[†] Peter K. Dornan,[†] Hasan A. Khan,[†] Tom K. Woo,*[,‡] and Vy M. Dong*[,†]

*Department of Chemistry, University of Toronto, 80 St. George Street, Toronto, Ontario, M5S 3H6, Canada, and Centre for Catalysis Research and Innovation, Department of Chemistry, University of Ottawa, Ottawa, Ontario, K1N 6N5, Canada*

Received August 27, 2008; E-mail: vdong@chem.utoronto.ca

***Abstract:*** [Rh((*R*)-DTBM-SEGPHOS)]$BF_4$ catalyzes the intramolecular hydroacylation of ketones to afford seven-membered lactones in large enantiomeric excess. Herein, we present a combined experimental and theoretical study to elucidate the mechanism and origin of selectivity in this C−H bond activation process. Evidence is presented for a mechanistic pathway involving three key steps: (1) rhodium(I) oxidative addition into the aldehyde C−H bond, (2) insertion of the ketone C═O double bond into the rhodium hydride, and (3) C−O bond-forming reductive elimination. Kinetic isotope effects and Hammett plot studies support that ketone insertion is the turnover-limiting step. Detailed kinetic experiments were performed using both 1,3-bis(diphenylphosphino)propane (dppp) and (*R*)-DTBM-SEGPHOS as ligands. With dppp, the keto-aldehyde substrate assists in dissociating a dimeric precatalyst **8** and binds an active monomeric catalyst **9**. With [Rh((*R*)-DTBM-SEGPHOS)]$BF_4$, there is no induction period and both substrate and product inhibition are observed. In addition, competitive decarbonylation produces a catalytically inactive rhodium carbonyl species that accumulates over the course of the reaction. Both mechanisms were modeled with a kinetics simulation program, and the models were consistent with the experimental data. Density functional theory calculations were performed to understand more elusive details of this transformation. These simulations support that the ketone insertion step has the highest energy transition state and reveal an unexpected interaction between the carbonyl-oxygen lone pair and a Rh d-orbital in this transition state structure. Finally, a model based on the calculated transition-state geometry is proposed to rationalize the absolute sense of enantioinduction observed using (*R*)-DTBM-SEGPHOS as the chiral ligand.

## Introduction

The stereoselective oxidation of carbon−hydrogen bonds is a challenging goal that has inspired the discovery of new and more efficient strategies for organic synthesis. The selective functionalization of aldehyde C−H bonds has been an especially active and fruitful area of research. A diverse range of catalysts, including organocatalysts,[1] metal alkoxides,[2] and transition metal complexes,[3] can promote the functionalization of aldehydic C−H bonds. These catalysts generate structurally fascinating intermediates that react via drastically distinct mechanistic pathways. For example, *N*-heterocyclic carbenes transform aldehydes into acyl anion equivalents by way of the nucleophilic Breslow intermediate.[4] On the other hand, aluminum alkoxides promote the conversion of aldehydes into hydride equivalents during the Tishchenko process,[1,5] while rhodium(I) complexes undergo oxidative addition with aldehydes to produce acyl rhodium(III) hydride intermediates.[6] These diverse mechanistic paradigms guide the development of many useful catalysts and transformations. A number of stereoselective and new variants of the benzoin condensation,[7] the Stetter reaction,[8] the Tishchenko dimerization,[9] and the hydroacylation of alkenes[3] have been achieved. Consequently, understanding the mechanism and origin of stereoselectivity in these processes is critical to broadening their scope and applicability.

Since Tsuji's original report of the rhodium-mediated decarbonylation of aldehydes,[6] the Rh-catalyzed activation of formyl C−H bonds has been used to develop hydroacylation of olefins and alkynes,[3,10] as well as formal cycloadditions of Rh acyl alkyl species.[11] In contrast, only isolated examples of transition metal-catalyzed hydroacylation of aldehydes[12] and one organocatalyzed hydroacylation of activated ketones[13] have been reported. The transition metal-catalyzed hydroacylation of

[†] University of Toronto.
[‡] University of Ottawa.

(1) Johnson, J. S. *Angew. Chem., Int. Ed.* **2004**, *43*, 1326.
(2) Tishchenko, V. E. *J. Russ. Phys. Chem. Soc.* **1906**, *38*, 482.
(3) Fu, G. C. In *Modern Rhodium-Catalyzed Reactions*; Evans, P. A., Ed.; Wiley-VCH: New York, 2005; pp 79−91, and references therein.
(4) Breslow, R. *J. Am. Chem. Soc.* **1958**, *80*, 3719.
(5) Ogata, Y.; Kawasaki, A.; Kishi, I. *Tetrahedron* **1967**, *23*, 825.
(6) Tsuji, J.; Ono, K. *Tetrahedron Lett.* **1965**, 3969.
(7) Enders, D.; Balensiefer, T. *Acc. Chem. Res.* **2004**, *37*, 534.
(8) Marion, N.; Diez-Gonzalez, S.; Nolan, I. P. *Angew. Chem., Int. Ed.* **2007**, *46*, 2988.
(9) (a) Mahrwald, R. *Curr. Org. Chem.* **2003**, *7*, 1713. (b) Hsu, J.-L.; Fang, J.-M. *J. Org. Chem.* **2001**, *66*, 8573.
(10) (a) Ritleng, V.; Sirlin, C.; Pfeffer, M. *Chem. Rev.* **2002**, *102*, 1731. (b) Jun, C. H.; Jo, E. A.; Park, J. W. *Eur. J. Org. Chem.* **2007**, *72*, 1869. (c) James, B. R.; Young, C. G. *J. Chem. Soc., Chem. Commun.* **1983**, 1215.

  

***Scheme 1.*** Mechanism-Based Design for the Ketone Hydroacylation

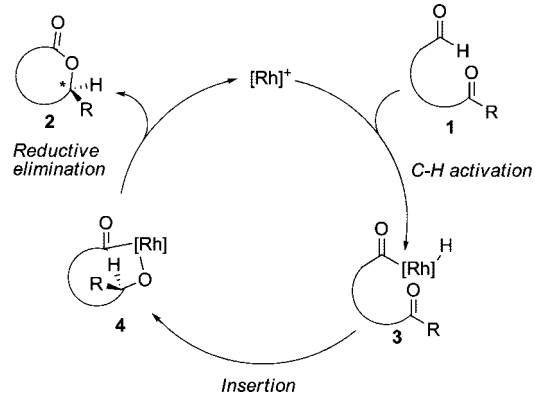


ketones has been virtually unexplored.[12a] Our group recently reported the first example of an enantioselective Rh-catalyzed hydroacylation of ketones.[14] By using a model substrate **1** derived from salicylaldehyde, we were able to produce chiral benzodioxepinones **2** in high yield and with excellent enantioselectivities (≥99% ee) (eq 1). In contrast to conventional methods known for making lactones, this strategy avoids wasteful preactivation of the substrate and use of stoichiometric reagents.[15] Our atom economical route to forming chiral lactones is mechanistically intriguing because the aldehyde is oxidized as the ketone is concomitantly reduced. Furthermore, this approach is amenable to enantioselective catalysis.

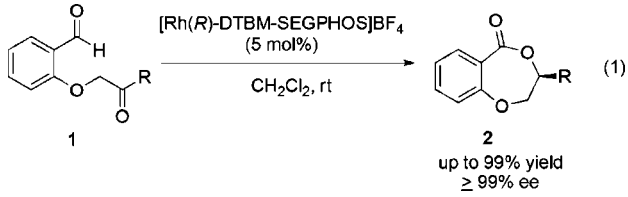


Our ketone-hydroacylation was designed on the basis of the mechanistic hypothesis illustrated in Scheme 1. We envisioned that a Rh(I) catalyst could undergo oxidative addition to an aldehyde to form an acyl-Rh(III) hydride species **3**. Insertion of the C═O bond of the ketone into this rhodium hydride would afford organorhodium metallacycle **4**. Reductive elimination would form the C−O bond and furnish the desired lactone product **2**. While the mechanism of olefin hydroacylation has been extensively studied,[16] the corresponding carbonyl hydroacylation is not well understood. In this article, we present experimental and theoretical studies to elucidate the mechanistic details of the transformation. In particular, we were interested in investigating the nature of the active catalysts, the kinetic profile for this transformation, the role of the ether oxygen, the coordination geometry of the reactive intermediates, and the origin of high enantioselectivity.

***Table 1.*** Catalyst Screening for Hydroacylation of Ketones

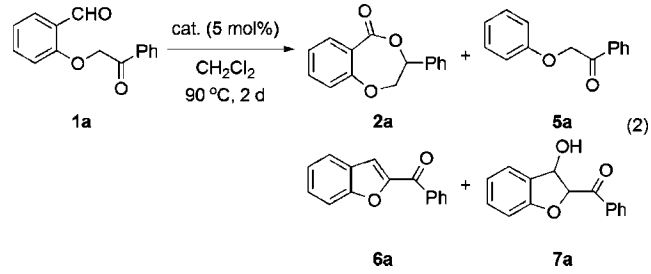


| | | yield (%)[a] | | | | |
|---|---|---|---|---|---|---|
| entry | catalyst | 2a | 5a | 6a | 7a | 1a |
| 1 | none | – | – | – | 8 | 92 |
| 2 | $[Rh(PPh_3)_3Cl]$ | – | 5 | 11 | 16 | 68 |
| 3 | $Ru_3(CO)_{12}$ | – | 3 | 4 | 3 | 90 |
| 4[b] | $Pd(PPh_3)_4$ | – | – | – | 33 | 67 |
| 5 | $[Rh(COD)_2]BF_4$ + dppp | 17 | – | – | – | 83 |
| 6[c] | $[Rh(dppp)]_2(BF4)_2$ | 96[d] | – | – | – | – |

[a] NMR yield. [b] 3 days, toluene, 110 °C. [c] 2 h, rt. [d] Isolated yield.

## Results and Discussion

**Reaction Optimization and Scope.** With this design in mind, we initially investigated a number of transition metal catalysts known to undergo oxidative addition to aldehydic C−H bonds.[6,17] For the model substrate, we chose readily available keto-aldehyde **1a** because it contains an ether oxygen that can coordinate to the metal center; on the basis of previous studies, such coordination is known to facilitate hydroacylation over competitive decarbonylation.[18] In the absence of any catalyst, a cyclization occurred to provide aldol product **7a** to a small extent (8%, Table 1, entry 1). The use of Wilkinson's catalyst, $Ru_3(CO)_{12}$ and $Pd(PPh_3)_4$ resulted in various amounts of the competing decarbonylation product **5a** and the aldol condensation products **6a** and **7a** (entries 2−4). However, studies with $[Rh(COD)_2]BF_4$ and dppp resulted in the desired lactone **2a** in 17% yield (entry 5). We reasoned that the sluggish reactivity of the $[Rh(COD)_2]BF_4$ + dppp results from competitive binding of the cyclooctadiene ligand to Rh (entry 2). Gratifyingly, the use of $[Rh(dppp)]_2(BF_4)_2$, prepared via the hydrogenation of $[Rh(NBD)_2]BF_4$ (NBD = norbornadiene) in the presence of dppp, resulted in complete conversion to **2a** with no byproduct resulting from decarbonylation or aldol side reactions (96% yield, entry 6).

**Bite Angle Effect.** Using cationic Rh(I), we examined a series of diphosphine ligands that have similar electronic properties to dppp but are expected to differ in their corresponding bite angles (Table 2).[19] The literature values for related metal

(11) (a) Tanaka, K.; Fu, G. C. *Org. Lett.* **2002**, *4*, 933. (b) Kundu, K.; McCullagh, J. V.; Morehead, A. T., Jr. *J. Am. Chem. Soc.* **2005**, *127*, 16042. (c) Tanaka, K.; Hojo, D.; Shoji, T.; Hagiwara, Y.; Hirano, M. *Org. Lett.* **2007**, *9*, 2059. (d) Hojo, D.; Noguchi, K.; Hirano, M.; Tanaka, K. *Angew. Chem., Int. Ed.* **2008**, *47*, 5820.
(12) (a) Bergens, S. H.; Fairlie, D. P.; Bosnich, B. *Organometallics* **1990**, *9*, 566. (b) Fuji, K.; Morimoto, T.; Tsutsumi, K.; Kakiuchi, K. *Chem. Commun.* **2005**, 3295. (c) Horino, H.; Ito, T.; Yamamoto, A. *Chem. Lett.* **1978**, 17. (d) Ozawa, F.; Yamagami, I.; Yamamoto, A. *J. Organomet. Chem.* **1994**, *473*, 265.
(13) Chan, A.; Scheidt, K. A. *J. Am. Chem. Soc.* **2006**, *128*, 4558.
(14) Shen, Z.; Khan, H. A.; Dong, V. M. *J. Am. Chem. Soc.* **2008**, *130*, 2916.
(15) Parenty, A.; Moreau, X.; Campagne, J. M. *Chem. Rev.* **2006**, *106*, 911.
(16) (a) Fairlie, D. P.; Bosnich, B. *Organometallics* **1988**, *7*, 946. (b) Barnhart, R. W.; Bosnich, B. *Organometallics* **1995**, *14*, 4343. (c) Lenges, C. P.; White, P. S.; Brookhart, M. *J. Am. Chem. Soc.* **1998**, *120*, 6965. (d) Roy, A. H.; Lenges, C. P.; Brookhart, M. *J. Am. Chem. Soc.* **2007**, *129*, 2082. (e) Hyatt, I. F. D.; Anderson, H. K.; Morehead, A. T.; Sargent, A. L. *Organometallics* **2008**, *27*, 135.
(17) Kondo, T.; Tsuji, Y.; Watanabe, Y. *Tetrahedron Lett.* **1987**, *28*, 6229.
(18) (a) Moxham, G. L.; Randell-Sly, H. E.; Brayshaw, S. K.; Woodward, R. L.; Weller, A. S.; Willis, M. C. *Angew. Chem., Int. Ed.* **2006**, *45*, 7618. (b) Imai, M.; Tanaka, M.; Nagumo, S.; Kawahara, N.; Suemune, H. *J. Org. Chem.* **2007**, *72*, 2543. (c) Jun, C.-H.; Moon, C. W.; Lee, D.-Y. *Chem. Eur. J.* **2002**, *8*, 2422, and references cited therein.
(19) (a) Casey, C. P.; Whiteker, G. T. *Isr. J. Chem.* **1990**, *30*, 299. (b) Achord, P. D.; Kiprof, P.; Barker, B. *J. Mol. Struct.* **2008**, *849*, 103.

***Table 2.*** Screening of Diphosphine Ligands with Varying Bite Angles

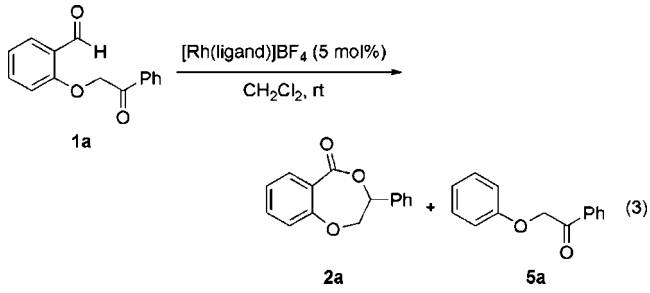


| entry | ligand | yield **2a** (%)[a] | yield **5a** (%)[a] | bite angle |
|---|---|---|---|---|
| 1 | dppm | <1 | <1 | 75.4[b] |
| 2 | dppe | 58 | 15 | 86.3,[b] 85.8[c] |
| 3 | dppp | 100[d] | <1 | 95.5,[b] 95[e] |
| 4 | dppb | 98 | 2 | 98.6,[b] 99[e] |
| 5 | dppf | <1 | <1 | 100.3,[b] 101.2[c] |

[a] Yield by $^1$H NMR after 24 h. [b] Calculated at the B3LYP/LACV3P** level, see Supporting Information for details. [c] Literature bite angles for square-planar Pd(diphosphine)(1,1-dimethylallyl) complexes from X-ray crystallography.[21] [d] Complete conversion after 4 h. [e] Reported bite angle for Pd(diphosphine)(1-methylallyl) calculated at the PM3 level.[22]

diphosphine complexes and calculated values for Rh(diphosphine)$^+$ (see Supporting Information for details) are listed in Table 2. Dppm (1,1-bis(diphenylphosphino)methane) forms the smallest bite angle with the rhodium center, followed by dppe (1,2-bis(diphenylphosphino)ethane), dppp, and dppb (1,4-bis(diphenylphosphino)butane). As summarized in Table 2, dppp provided optimal reactivity as complete conversion was observed after 4 h. Dppb was also effective, promoting 98% conversion after 24 h. However, the reaction efficiency dropped precipitously with smaller bite angles: with dppe, only 58% conversion could be achieved, and with dppm, no desired hydroacylation was observed. Decarbonylation was observed in the cases of dppe (entry 2) and dppb (entry 4). Dppf (1,1′-bis(diphenylphosphine)ferrocene) was ineffective at promoting hydroacylation of **1a**. The results of Table 2 suggest that ligand bite angle affects the rates of hydroacylation and decarbonylation. However, bite angle influences both processes to different degrees, considering that no decarbonylation was observed with dppp, which is an extremely effective ligand for hydroacylation. The precise mechanism by which bite angle influences these two processes is difficult to elucidate, especially considering that bite angle is known to impart both steric and electronic influences on metal catalysts.[20] However, it should be noted that decarbonylation requires dissociation of a ligand to open a coordination site (Figure 13, **TS-4**, vide infra), and the steric properties of the ligand are expected to affect this process.

**Scope Studies.** A variety of substrates, including both alkyl- and arene-substituted ketones, underwent hydroacylation in high yields (89−99%) and with short reaction times (1.2−12 h) (Table 3, entries 1−13), with the exception of furyl- and thienyl-substituted ketones (78% and 37%, respectively) (entries 14 and 15). With these heteroaromatic ketones, benzofuran side-

***Table 3.*** Hydroacylation of Substituted Keto-Aldehydes Using $[Rh(dppp)]_2(BF_4)_2$[a]

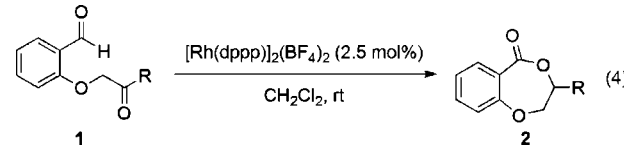


| entry | R | time (h) | % yield[b] |
|---|---|---|---|
| 1 | Ph (**1a**) | 4 | 94 |
| 2 | 4-$CF_3$−Ph (**1b**) | 1.2 | >99 |
| 3 | 4-C(O)OMe-Ph (**1c**) | 1.5 | 98 |
| 4 | 4-Cl-Ph (**1d**) | 3.5 | 95 |
| 5 | 4-F-Ph (**1e**) | 1.2 | 96 |
| 6 | 4-$CH_3$−Ph (**1f**) | 5 | >99 |
| 7 | 4-OMe-Ph (**1g**) | 12 | 89 |
| 8 | 2-naphthyl (**1h**) | 4.5 | 91 |
| 9 | *n*-Bu (**1i**) | 9 | 94 |
| 10 | *i*-Pr (**1j**) | 3.7 | 95 |
| 11 | *t*-Bu (**1k**) | 3.5 | 94 |
| 12 | Bn (**1l**) | 9 | 92 |
| 13 | Me (**1m**) | 10 | >99 |
| 14 | 2-furyl (**1n**) | 20 | 78 |
| 15 | 2-thiophenyl (**1o**) | 28 | 37 |

[a] Conditions: substrate (0.2 mmol), $[Rh(dppp)]_2(BF_4)_2$ (2.5 mol%) in degassed $CH_2Cl_2$ (2 mL) at rt. [b] Isolated yield.

products (analogous to **6a**, Table 1) could be observed due to competitive intramolecular aldol condensation.

The hydroacylation of α-substituted keto-aldehydes **1p** and **1q** resulted in high yields (86−89%) of the corresponding lactones **2p** and **2q** with excellent diastereocontrol (eqs 5 and 6). By $^1$H NMR analysis, we discovered that only the cis diastereomer of lactone **2p** could be observed. The cis diastereoselectivity was confirmed upon obtaining the molecular structure of **2q** from single crystal X-ray crystallography as depicted in eq 6. These examples highlight the potential of using diastereoselective ketone hydroacylation as a strategy in complex molecule synthesis.

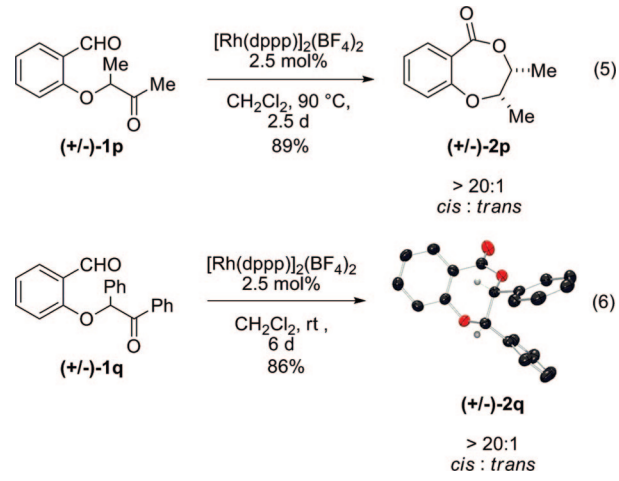


**Enantioselective Catalysis.** Next, we evaluated a number of chiral diphosphine ligands to achieve an enantioselective transformation (Table 4). Although (*R*)-BINAP is an effective ligand for the enantioselective hydroacylation of alkenes,[3] this privileged ligand[23] was ineffective at promoting the hydroacylation of ketones. By evaluating a series of ligands based on the MeOBIPHEP framework, we observed a remarkable trend relating phosphine basicity to hydroacylation efficiency. The

(20) Freixa, Z.; van Leeuwen, P. W. N. M. *Dalton Trans.* **2003**, 1890.
(21) van Haaren, R. J.; Goubitz, K.; Fraanje, J.; van Strijdonck, G. P. F.; Oevering, H.; Coussens, B.; Reek, J. N. H.; Kamer, P. C. J.; van Leeuwen, P. W. N. M. *Inorg. Chem.* **2001**, *40*, 3363.
(22) van Haaren, R. J.; Oevering, H.; Coussens, B. B.; van Strijdonck, G. P. F.; Reek, J. N. H.; Kamer, P. C. J.; van Leeuwen, P.W.N.M. *Eur. J. Inorg. Chem.* **1999**, 1237.

***Table 4.*** Chiral Ligand Screen

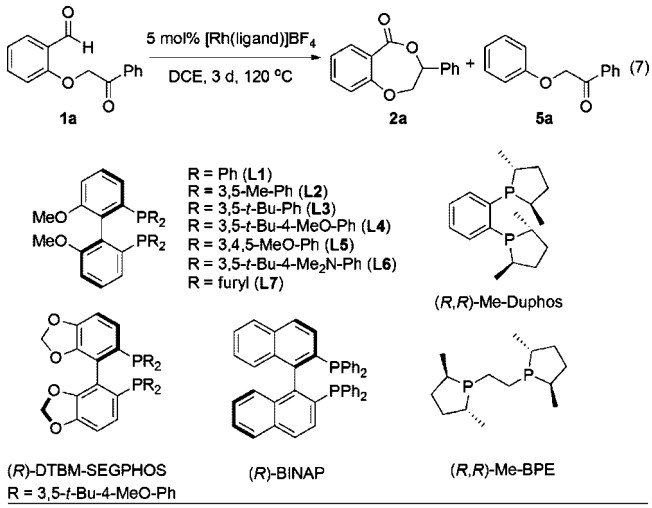


| entry | ligand | **2a** (%)[a] | ee (%)[b] | **5a** (%)[c] |
|---|---|---|---|---|
| 1[d] | (*R*)-BINAP | – | – | 19 |
| 2[d] | **L1** | <1 | – | 13 |
| 3 | **L1** | 2 | n/a | 98 |
| 4 | **L2** | 5 | n/a | 93 |
| 5 | **L3** | 45 | 96 | 38 |
| 6 | **L4** | 63 | 95 | 31 |
| 7 | (*R*)-DTBM-SEGPHOS | 76 | 96 | 22 |
| 8 | **L5** | 28 | 95 | 70 |
| 9 | **L6** | 22 | 85 | 43 |
| 10 | **L7** | – | – | 8 |
| 11 | (*R*,*R*)-Me-Duphos | 95 | 82 | <5 |
| 12 | (*R*,*R*)-Me-BPE | 46 | 76 | 6 |

[a] Yields are based on integration by $^1$H NMR relative to starting material peaks. [b] Determined by chiral HPLC. [c] Decarbonylated product yields based on $^1$H NMR integration relative to product peaks. [d] 90 °C.

more electron-rich phosphine ligands appear to progessively favor hydroacylation over decarbonylation (compare ligands **L1** to **L4**, entries 4−6). (*R*)-Ph-MeOBIPHEP (**L1**) was ineffective at promoting hydroacylation; at 120 °C, the decarbonylated byproduct **5a** was formed in 98% yield with a trace amount of desired product **2a** (<2% yield) (entry 3). In contrast, with ligand **L4**, the desired lactone **2a** was isolated in 63% yield and 99% ee, in addition to decarbonylated product **5a** (31% yield) (entry 6). With (*R*)-DTBM-SEGPHOS, a ligand more electron-rich than **L4**, we were able to obtain **2a** in 76% yield while maintaining high enantiomeric excess (96% ee) and decreasing the amount of decarbonylation byproduct **5a** (22% yield). Other MeOBIPHEP-based ligands were less effective: ligands **L5**, **L6**, and **L7**, (R = 3,4,5-MeO-Ph, 3,5-*t*-Bu-4-Me$_2$N-Ph-, and furyl, respectively) provided **2a** in 28%, 22%, and 0% yield, respectively. The chiral alkyl-substituted diphoshine ligand (*R*,*R*)-Me-Duphos provided excellent yield of **2a** (95% yield) and 82% ee (entry 11). (*R*,*R*)-Me-BPE, the most basic ligand in this study, was less reactive and selective (46% yield, 76% ee, entry 12).

At room temperature in $CH_2Cl_2$, catalyst [Rh((*R*)-DTBM-SEGPHOS)]$BF_4$ provided optimal results (92% yield of **2a**, 99% ee, Table 5, entry 1). Under these conditions, a wide variety of substrates with arene- and alkyl-substituted ketones were tolerated (Table 5). Ketones bearing electron-poor arene substituents were transformed to their corresponding lactones in excellent yield and enantiomeric excess (97−98% yield, 99% ee) with little decarbonylation side-product (1−1.5%) (entries 2 and 3). In comparison, electron-rich arene-substituted substrates underwent hydroacylation more slowly (entries 6 and 7): the *p*-tolyl-substituted substrate **1f** was converted to the corresponding lactone selectively (99% ee) albeit in moderate yield (50%) (entry 6), and the *p*-methoxyphenyl-substituted substrate **1g** underwent hydroacylation with poor efficiency and low enantioselectivity (14% yield and 32% ee) (entry 7). Compared to the arene-substituted ketones, asymmetric hydroacylation of aliphatic ketones occurred in relatively higher yields, higher enantioselectivities, and shorter reaction times (entries 9−13). With the exception of the methyl-substituted ketone **1m** case (entry 13), no competing decarbonylation was observed, and essentially one enantiomer of the corresponding lactones were formed (>99% ee) (entries 9−12). Heteroarene-substituted ketones were not well-tolerated; a furyl substituted substrate (entry 14) was transformed in a very poor yield (7%) with a significant amount of the decarbonylation byproduct (41%), while a thiophene substituted ketone (entry 15) formed only the decarbonylated byproduct in 73% yield.

***Table 5.*** Hydroacylation of Substituted Keto-Aldehydes Using [Rh((*R*)-DTBM-SEGPHOS)]$BF_4$

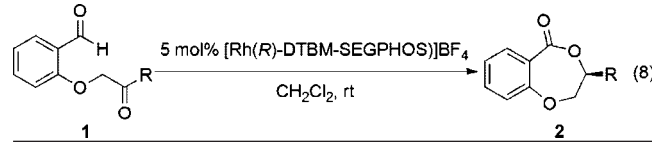


| entry | R | **2** (%)[a] | time (days) | ee (%)[b] | **5** (%)[c] |
|---|---|---|---|---|---|
| 1 | Ph (**1a**) | 92 | 3 | 99 | 7 |
| 2 | 4-$CF_3$−Ph (**1b**) | 97 | 2 | 99 | 1 |
| 3 | 4-COOMe-Ph (**1c**) | 98 | 2 | 99 | 1.5 |
| 4 | 4-Cl-Ph (**1d**) | 89 | 2 | 99 | 7 |
| 5 | 4-F-Ph (**1e**) | 84 | 3 | 99 | 7 |
| 6 | 4-$CH_3$−Ph (**1f**) | 50 | 6 | 99 | 8 |
| 7 | 4-MeO-Ph (**1g**) | 14 | 6 | 32 | 9 |
| 8 | 2-naphthyl (**1h**) | 85 | 2 | 99 | 9 |
| 9 | *n*-Bu (**1i**) | 99 | 2 | >99 | 0 |
| 10 | *i*-Pr (**1j**) | 98 | 1.5 | >99 | 0 |
| 11 | *t*-Bu (**1k**) | 94 | 1.5 | >99 | 0 |
| 12 | Bn (**1l**) | 93 | 3.5 | >99 | 0 |
| 13 | Me (**1m**) | 91 | 2 | 99 | 6 |
| 14[d] | 2-furyl (**1n**) | 7 | 5 | ND[e] | 41 |
| 15[d] | 2-thiophenyl (**1o**) | – | 4 | ND[e] | 73 |

[a] Isolated yield. [b] Determined by chiral HPLC. [c] The yield of decarbonylated product is based on $^1$H NMR integration relative to product and staring material peaks. [d] 90 °C in sealed tube. [e] Not determined.

In summary, we have identified two effective Rh−diphosphine complexes for ketone hydroacylation: [Rh(dppp)]$_2$(BF$_4$)$_2$ and [Rh((*R*)-DTBM-SEGPHOS)]$BF_4$. The former provides rapid and complete conversion to chiral benzodioxepinones with no observed byproducts and excellent diastereoselectivity with α-chiral ketones, while the latter is a highly enantioselective catalyst. Interestingly, these two catalytic systems displayed significantly distinct kinetic profiles. As such, we decided to probe the mechanistic details of ketone hydroacylation using both catalysts.

**Mechanism of Hydroacylation with [Rh(dppp)]$_2$(BF$_4$)$_2$.** On the basis of various experimental studies and literature precedence, we propose the mechanism shown in Scheme 2. Substrate **1a** mediates slow dissociation of the dimeric precatalyst **8** to give a monomer−substrate complex **9**. Complex **9** undergoes a fast and reversible oxidative addition to the C−H bond of the aldehyde. Results of a kinetic isotope study and Hammett plot

(23) Yoon, T. P.; Jacobsen, E. N. *Science* **2003**, *299*, 1691.

***Scheme 2.*** Proposed Mechanism for the Hydroacylation of **1a** with $[Rh(dppp)]_2(BF_4)_2$

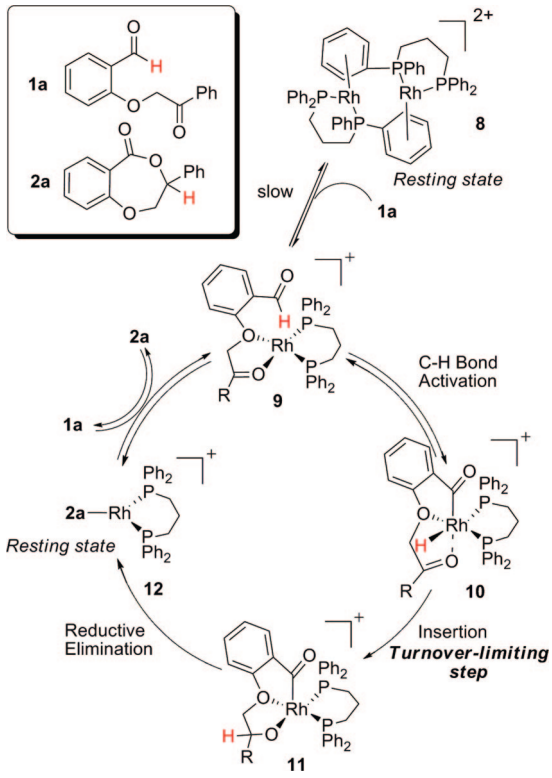


suggest that the turnover-limiting step is insertion of the ketone carbonyl into the rhodium hydride **10** to provide intermediate **11**. The irreversible reductive elimination of **11** forms the lactone−Rh complex **12** (a catalyst resting state). To complete the catalytic cycle, another molecule of the substrate can displace the product from complex **12** to form the substrate-bound complex **9**. Both dimer dissociation and catalyst turnover influence the overall rate. The experimental observations that led us to this proposed mechanism are discussed in more detail below.

**Crossover Experiment.** In accord with known Rh(I)-catalyzed hydroacylation reactions,[16] we hypothesized that the mechanism occurs via an intramolecular process. To support this hypothesis, we performed a crossover experiment using a mixture of the deuterium-labeled substrate **1a-D** and the protio substrate **1k** and observed formation of the corresponding lactone products **2a-D** and **2k** (Scheme 3). Since substrates **1a** and **1k** show similar reactivity (Table 3), absence of crossover products **2a** and **2k-D** supports a mechanism where hydride transfer occurs *intra*molecularly. These results disfavor alternative intermolecular mechanisms (i.e., the Rh−H derived from one substrate reducing the ketone-carbonyl of another substrate).

**NMR Studies (dppp).** Initial studies focused on monitoring the stoichiometric reaction of $[Rh(dppp)]_2(BF_4)_2$ **8** with substrate **1a** by both $^1H$ and $^{31}P$ NMR at low temperature. Bosnich previously reported that $[Rh(dppp)]^+$ exists as a diastereomeric mixture of arene-bridged dimers in noncoordinating solvents such as $CH_2Cl_2$ or $CH_3NO_2$.[16a] In accord with Bosnich's observations, we observed a 1:1 mixture of complexes by $^{31}P$ NMR that can be attributed to the meso and chiral dimeric forms of $[Rh(dppp)]_2^{2+}$ in $CH_2Cl_2$ (Figure 1). While the analogous dimer of $[Rh(dppe)]^+$ has been confirmed in the solid state,[24] the dimeric forms of $[Rh(dppp)]^+$ were characterized in solution by $^{31}P$ NMR studies.[16a] We have performed theoretical calculations to obtain optimized structures of the proposed meso **8a** and racemic dimers **8b**, as shown in Figure 1.[25]

The reaction of **1a** with 2.5 mol % $[Rh(dppp)]_2(BF_4)_2$ (**8a** and **8b**) was monitored by $^1H$ and $^{31}P$ NMR from −80 to 0 °C (by increasing increments of 20 °C) in an attempt to observe putative reaction intermediates. This experiment showed that the dimeric Rh species **8a** and **8b** were stable from −80 to −20 °C. At 0 °C, a new signal ($\delta = 25.8$ ppm, $J = 191$ Hz) appeared in the spectrum as a doublet upfield of the signals corresponding to the Rh dimers. After complete consumption of the ketoaldehyde **1a**, ~32% of the dimer had been converted to this complex (Figure 2). We attribute this resting state to a three-coordinate Rh-complex **12** (where product is bound to Rh with enough rotational freedom to allow for equivalent phosphines). We have ruled out structures featuring two products bound to Rh by performing experiments where two different lactone products were added to the catalyst precursor $Rh(NBD)_2BF_4$ and then hydrogenated as usual (see Supporting Information for details). In the presence of product **2a** and **2c**, two doublets were observed in the $^{31}P$ NMR spectrum ($\delta = 25.8$ ppm, $J(Rh-P) = 190$ Hz; $\delta = 26.5$ ppm, $J(Rh-P) = 192$ Hz), along with a small amount of the dimeric complexes **8**. The upfield doublet matches the doublet which we previously attributed to complex **12**, while the downfield doublet is consistent with a Rh-complex coordinated to product **2c**.[26] Importantly, no mixed species were observed suggesting that only 1 equivalent of product binds to Rh.

Next, the reaction of **1a** with stoichiometric $[Rh(dppp)]_2(BF_4)_2$ **8a** and **8b** was also monitored by $^1H$ and $^{31}P$ NMR from −80 to 0 °C. The dimeric species was unreactive in the low-temperature range.[27] After 90 min at 0 °C, ~6% product was observed by $^1H$ NMR, and after 1 min at room temperature, 66% product was formed. At this point, the $^{31}P$ NMR spectrum indicated a large amount of dimer along with 34% of complex **12**. Importantly, signals corresponding to late metal hydrides (0 to −60 ppm)[28] were not observed.

On the basis of these NMR studies, we postulate that the meso and racemic dimers **8a** and **8b** are inactive precatalysts that must dissociate to form an active monomeric catalyst. Bosnich has suggested a similar dimer-splitting step in his mechanistic study on the hydroacylation of 4-pentenal by $[Rh(dppe)]_2^{2+}$.[16a] In this report, he noted the dimer is a coordinatively saturated 18-electron species and therefore, most likely a precatalyst. Plotting $k_{obs}$ versus catalyst concentration revealed a fractional order fit of 0.67 (Figure 3). A half-order kinetic dependence would be expected in a reaction involving slow dissociation of a dimeric precatalyst to an active monomer, whereas a first-order kinetic dependence would be expected if both the ground-state and the transition structure are derived

(24) Halpern, J.; Riley, D. P.; Chan, A. S. C.; Pluth, J. J. *J. Am. Chem. Soc.* **1977**, *99*, 8055.
(25) At the B3LYP/lan2ldz level of theory (see Computational Study for details).
(26) The same result was obtained when **2a** and **2h** were used. Here three doublets were observed, ($\delta$ 25.8, $J(Rh-P) = 192$ Hz; $\delta$ 22.1, $J(Rh-P) = 191$ Hz; $\delta$ 21.9, $J(Rh-P) = 190$ Hz); however, the two upfield doublets are present when only **2h** is added, and thus are likely two binding modes of **2h**.
(27) At 0 °C, a small amount (3%) of an unidentified species was observed in the $^{31}P$ NMR spectrum.
(28) Crabtree, R. H. *The Organometallic Chemistry of the Transition Metals*, 3rd ed.; John Wiley and Sons, Inc: New York, 2001.

***Scheme 3.*** Crossover Experiment to Confirm Intramolecular Hydride Transfer

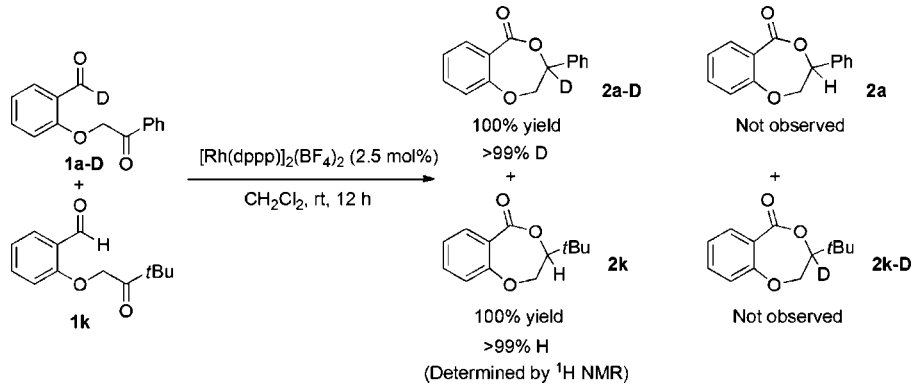


from monomeric catalyst species.[29] Dimers **8** and complex **12** are catalyst resting states observable by NMR analysis. Thus, the rates of dimer dissociation and catalyst turnover are both important in controlling the reaction rate.

To further support that substrate **1a** can facilitate the dissociation of the dimeric precatalyst, we prepared diketone analogue **1r** (see Supporting Information for details). Diketone **1r** should bind to dimer **8** in a similar manner to the substrate **1a**, but the resulting complex should be spectroscopically detectable as it is incapable of undergoing oxidative addition. Indeed, when 40 equiv of diketone **1r** were added to a 0.001 M solution of $[Rh(dppp)]_2(BF_4)_2$ in $CD_2Cl_2$, (eq 9), the $^{31}P$ NMR signals corresponding to **8a** and **8b** were observed to slowly disappear at room temperature (19% conversion after 30 min). After heating at 90 °C for 2 h, the dimer signals for **8a** and **8b** were completely absent and a new set of resonances were observed. We attribute these new signals to a mixture of three monomeric Rh species bound to **1r** with various modes of coordination (eq 9). One of these complexes has nonequivalent phosphine resonances (a pair of doublet of doublet signals ($\delta$ = 25.3 ppm, $J$(Rh−P) = 127 Hz, $J$(P−P) = 42 Hz; $\delta$ = 18.7 ppm, $J$(Rh−P) = 133 Hz, $J$(P−P) = 42 Hz)), while the other two species have equivalent phosphine resonances (two doublets ($\delta$ = 23.3 ppm, $J$(Rh−P) = 124 Hz, $\delta$ = 23.2 ppm, $J$(Rh−P) = 128 Hz)). A number of structures can be proposed that are consistent with the observed signals (e.g., four-coordinate Rh(I) complexes chelating to **1r** or three-coordinate[30] Rh(I) bound to **1r**). Although the exact nature of this mixture is elusive, this experiment demonstrates that dimer dissociation is facilitated by substrate binding and this process is relatively slow.

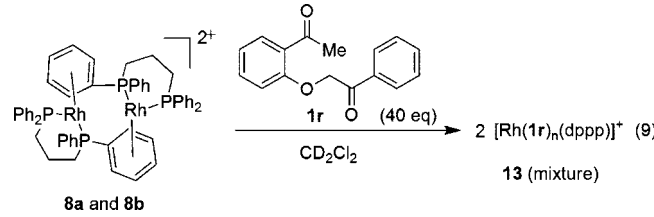


**Kinetics Studies (dppp).** After studying the resting states of the catalyst in solution, we turned our attention to the effect of substrate and product on the rate of reaction with $[Rh(dppp)]_2(BF_4)_2$. To determine the kinetic order in substrate **1a**, we measured the rate of reaction (after an apparent induction period) with various concentrations of the substrate. We were able to observe a first-order dependence of the rate on substrate concentration (Figure 5). Addition of 2 equivalents of product **2a** resulted in a 40% decrease in the observed rate of the reaction. Our observation of product inhibition is consistent with the accumulation of product-bound complex **12** by NMR analysis as discussed above. Notably, the observed rate of product formation remains constant until much higher conversion than would be expected given a typical first-order rate law. The kinetic profile shows a

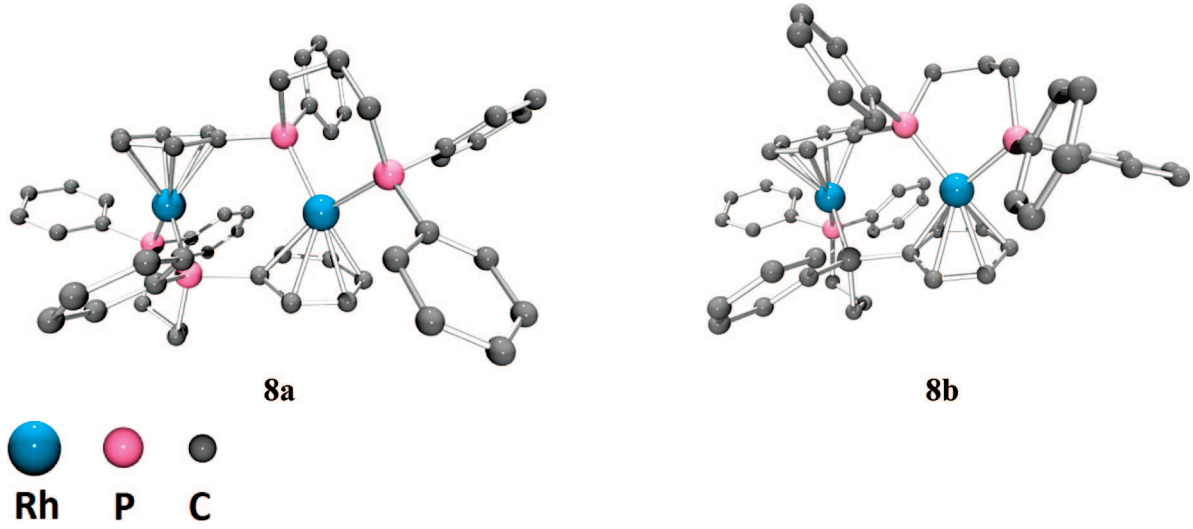


***Figure 1.*** DFT-optimized[25] structures for $[Rh(dppp)]_2^{2+}$. Left, meso diastereomer **8a**; right, chiral diastereomer **8b**.

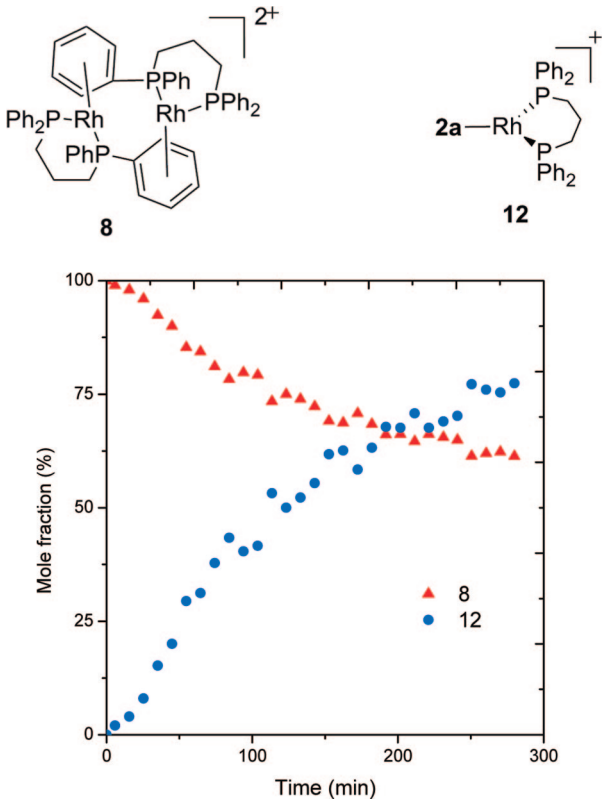


***Figure 2.*** Reaction of 0.1 M **1a** and 2.5 mol % $[Rh(dppp)]_2(BF_4)_2$, in $CD_2Cl_2$ monitored by $^{31}P$ NMR.

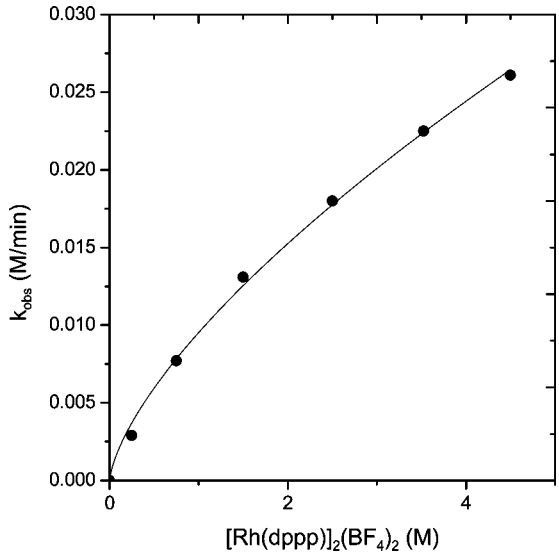


***Figure 3.*** Observed rate (measured after the initial induction period) versus catalyst concentration. The curve describes a nonlinear fit to the power function $k_{obs} = a[Rh(dppp)]_2(BF_4)_2]^b$ ($a = 0.0095 \pm 0.0003$; $b = 0.67 \pm 0.03$).

pronounced sigmoidal curve (Figure 5). An induction phase, followed by a relatively long interval where rate of product formation appears constant (up to ca. 60% conversion) is observed. This sigmoidal curve supports that the concentration of active catalyst increases over the course of the reaction due to slow dimer dissociation. This mechanistic scenario (Scheme 2) was modeled using the kinetics modeling

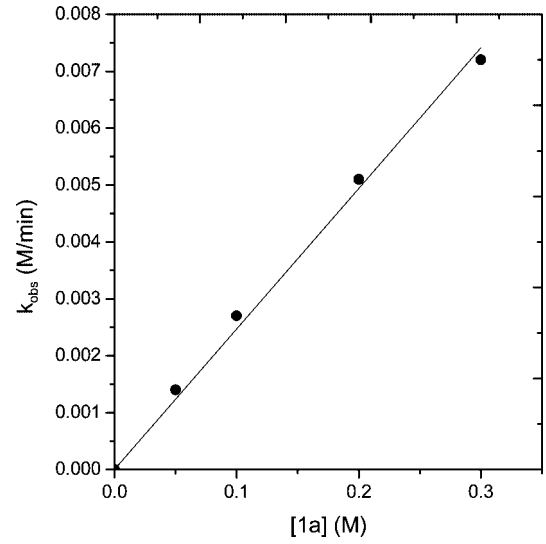


***Figure 4.*** Plot of $k_{obs}$ vs [**1a**] with $[Rh(dppp)]_2(BF_4)_2$ (0.0025 M). The curve describes a linear least-squares fit to $k_{obs} = m$[**1a**] ($m = 0.0247 \pm 0.0005$).

software package Copasi.[31] As illustrated in Figure 5, our proposed mechanism is consistent with the observed kinetic profile.

**Support for Turnover-Limiting Step.** The rate of a catalytic process can be influenced by a number of factors and steps. For example, in this study, dimer dissociation affects the rate by controlling the concentration of active catalyst in solution. To determine the turnover-limiting step in this ketone hydroacylation (i.e., the step with the highest energy transition state *within* the catalyst cycle) the H/D kinetic isotope effect (KIE) for substrate **1a** was examined with $[Rh(dppp)]_2(BF_4)_2$ (eq 11).

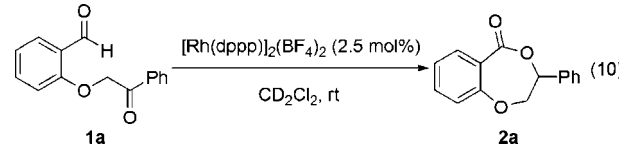


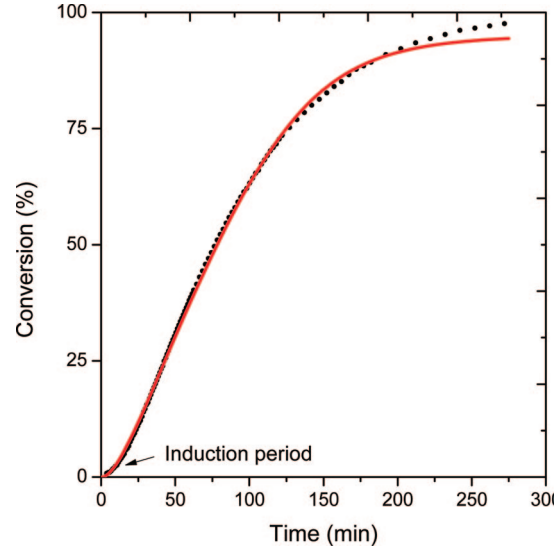


***Figure 5.*** Reaction profile for the hydroacylation of **1a** with $[Rh(dppp)]_2(BF_4)_2$ monitored by $^1H$ NMR (dotted line) and Copasi model fit (solid line) show sigmoidal curve.

As mentioned above, the rate constants were obtained from the slope of the linear region of the curve after the apparent induction period. The $k_H/k_D$ was determined to be 1.79 ± 0.06. Since the H/D atom is relatively far from the forming C−O bond, a negligible H/D KIE would be expected if reductive elimination were the turnover-limiting step.[32] Thus, the observed kinetic isotope effect suggests that reductive elimination is not the turnover-limiting step.[33]

A Hammett plot was constructed in order to determine the rate dependence on the electronic character of the ketone (Figure 6). The intramolecular hydroacylation of seven arylketones (**1a**−**g**), in the presence of 1.25 mol % $[Rh(dppp)]_2(BF_4)_2$, was monitored by $^1H$ NMR to obtain reaction rates (after the induction period). By plotting these rates versus $\sigma^+$,[34] a clear trend was observed with relatively electron-poor aryl ketones undergoing hydroacylation more rapidly. Linear regression of the Hammett plot yielded $\rho = +0.29 \pm 0.04$ with good correlation ($R^2 = 0.91$). However, care must be taken in interpreting this result because the electronic character of the ketone affects not only the rate of catalytic turnover, but also the rate of dimer dissociation to produce active catalyst. Since more electron-rich aryl ketones possess a more basic lone pair on the ketone and a more basic arene, they are also more effective at promoting dissociation of the dimeric form of the catalyst. Indeed, we can see this effect by examining the reaction profiles of the substrates in the Hammett plot. For example, as shown in Figure 7, substrate **1g** (*p*-OMe) does not show an induction period and initially reacts faster than substrate **1c** (*p*-COOMe). However, substrate **1c** does demonstrate a significant

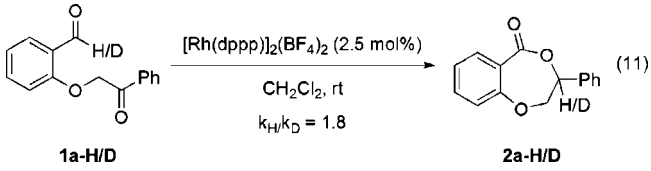


induction period and reacts much faster than **1g** after the induction period. This trend suggests that electron-rich substituents facilitate the dissociation of the dimer more effectively than electron-poor substituents, but electron-poor substituents preferentially accelerate the turnover-limiting step. The slope of the Hammett plot results from the combination of these two factors. Both the observed kinetic isotope effect and the Hammett study support insertion of the ketone into the rhodium hydride as the turnover-limiting step. This result represents a significant difference between the mechanism of our ketone hydroacylation and the related olefin hydroacylation; for olefin hydroacylation it is well established that reductive elimination is rate-determining.[16]

**Mechanism of Hydroacylation with [Rh((*R*)-DTBM-SEGPHOS)]$BF_4$.** On the basis of kinetic studies, NMR experiments, and

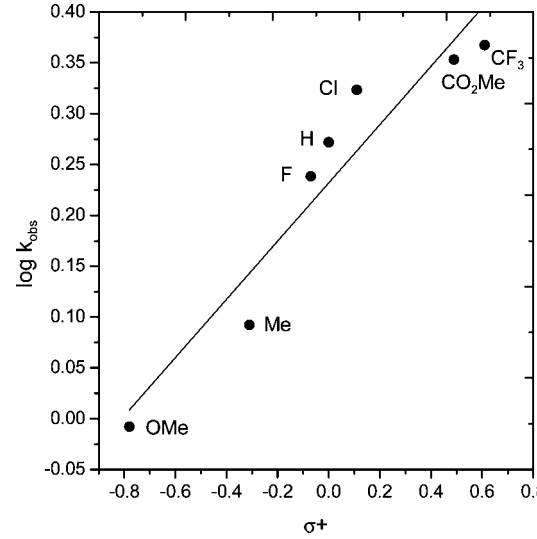


***Figure 6.*** Hammett plot for the hydroacylation of keto-aldehyde substrates **1a**−**g**. The curve describes a linear least-squares fit to log $k_{obs} = m\sigma^+ + b$ ($m = 0.29 \pm 0.04$; $b = 0.23 \pm 0.02$; $R^2 = 0.91$).

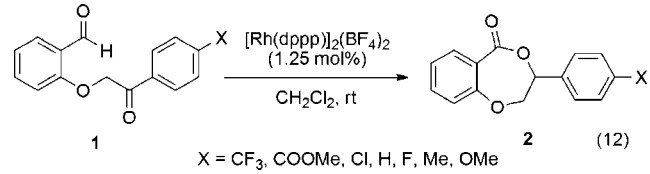


computational modeling, we propose the mechanism shown in Scheme 4 for the hydroacylation of **1a** with [Rh((*R*)-DTBM-SEGPHOS)]$BF_4$. In contrast to the mechanism proposed for dppp, the resting state of the catalyst is a monomeric Rh-

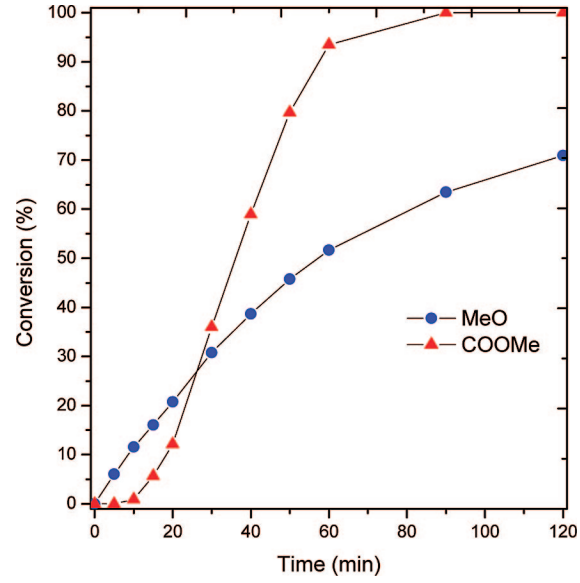


***Figure 7.*** Product formation as a function of time for substrates **1c** and **1g**.

(29) Collum, D. B.; McNeil, A. J.; Ramirez, A. *Angew. Chem., Int. Ed.* **2007**, *46*, 3002.
(30) Three-coordinate Rh(I) have been reported in the literature: (a) Yared, Y. W.; Miles, S. L.; Bau, R.; Reed, C. A. *J. Am. Chem. Soc.* **1977**, *99*, 7067. (b) Van Gaal, H. L. M.; Van Den Bekerom, F. L. A. *J. Organomet. Chem.* **1977**, *134*, 237. (c) Budzelaar, P. H. M.; de Gelder, R.; Gal, A. W. *Organometallics* **1988**, *17*, 4121.
(31) Hoops, S.; Sahle, S.; Gauges, R.; Lee, C.; Pahle, J.; Simus, N.; Singhal, M.; Xu, L.; Mendes, P.; Kummer, U. *Bioinformatics* **2006**, *22*, 3067.
(32) It is also possible that reversible insertion steps could lead to a pre-equilibrium isotope effect which would translate to different rates of rate-limiting reductive elimination based on different concentrations of the intermediate prior to reductive elimination. However, we believe this is unlikely since the observed $k_H/k_D = 1.8$ is large for a thermodynamic isotope effect:(a) Kogut, E.; Zeller, A.; Warren, T. H.; Strassner, T. *J. Am. Chem. Soc.* **2004**, *126*, 11984 Also see Computational Study for additional support for ketone insertion as the rate-determining step.
(33) A KIE of $k_H/k_D = 3.3 \pm 0.3$ was determined for the same substrate with [Rh(*R*)-DTBM-SEGPHOS]$(BF_4)$.
(34) Hansch, C.; Leo, A.; Taft, R. W. *Chem. Rev.* **1991**, *91*, 165.

***Scheme 4.*** Proposed Mechanism for [Rh((*R*)-DTBM-SEGPHOS)]$BF_4$-Catalyzed Hydroacylation of **1a**

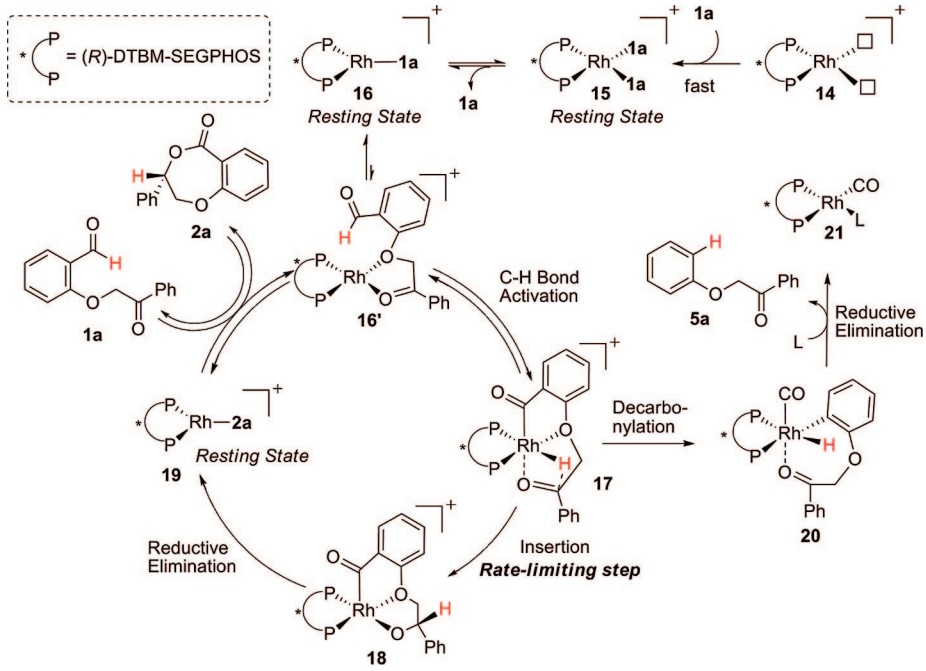


complex **15** (coordinated to two molecules of substrate **1a**). In order to undergo catalysis, one molecule of **1a** dissociates to form a three-coordinate complex **16**. In support of this mechanism, the substrate is observed to inhibit the reaction rate. While **16** can be observed by NMR, computational modeling suggests that the intermediate prior to oxidative insertion is a square-planar, four-coordinate Rh(I) complex **16′** (in which the ether oxygen is coordinated to Rh). Reversible C−H bond activation occurs to form **17** which undergoes rate-limiting insertion. Reductive elimination forms complex **19** from which another substrate molecule **1a** can displace the bound product **2a** and regenerate **16′**. In this catalytic system, decarbonylation is a kinetically competitive process that occurs subsequent to oxidative addition and ultimately leads to the formation of a Rh−CO complex **21** that is not an active catalyst.[16a] This mechanistic proposal is consistent with the experimental data and supported by computational studies as described below.

**NMR Studies ((*R*)-DTBM-SEGPHOS).** The $^{31}$P NMR spectrum of [Rh((*R*)-DTBM-SEGPHOS)]$BF_4$ (**14**) shows a simple doublet 53.2 ppm ($J_{Rh-P}$ = 208 Hz), which suggests that the catalyst is monomeric in solution. The phosphines couple only to rhodium and therefore, they are identical by symmetry and cannot be involved in bridging. In contrast to dppp, the steric bulk of the (*R*)-DTBM-SEGPHOS ligand prevents the Rh complex from forming a dimer. In solution, this catalyst is most likely solvated by two weakly coordinating dichloromethane molecules. When 25 equivalents of the substrate **2a** were added to the catalyst solution at room temperature in $CD_2Cl_2$, the $^{31}$P NMR peaks corresponding to [Rh((*R*)-DTBM-SEGPHOS)]$BF_4$ disappeared immediately and two new doublets of approximately equal intensity ($\delta$ = 53.7 ppm, $J$ = 199 Hz; $\delta$ = 39.7 ppm, $J$ = 202 Hz) were observed. We attribute these peaks to an equilibrium mixture of complex **15** and complex **16**, where **15** ($\delta$ 53.7) is a four-coordinate complex bound to *two* molecules of **2a** and **16** ($\delta$ 39.7) is a three-coordinate bound to *one* molecule of **2a**.

Initial experiments to study this proposed equilibrium were difficult to analyze due to rapid formation of product **2a** (which also binds competitively to Rh). Because the diketone analogue **1r** cannot undergo hydroacylation, we performed a model study. Upon addition of **1r** to a solution of catalyst in $CD_2Cl_2$, we observed two clean doublets with chemical shifts ($\delta$ 51.9, $J$ = 200 Hz; $\delta$ 40.0, $J$ = 200 Hz) similar to those attributed to complexes **15** and **16**. Importantly, by varying the concentration of **1r**, the relative intensity of these two peaks changed substantially; this change supports the existence of an equilibrium that is sensitive to substrate concentration. At higher concentrations of **1r**, the downfield doublet ($\delta$ 51.9) grew in relative intensity. On the basis of this model study, we propose that the analogous downfield doublet ($\delta$ 53.7) belongs to complex **15** which is bound to two substrate molecules and therefore, favored at higher substrate concentration.[35]

**Kinetic Studies ((*R*)-DTBM-SEGPHOS).** With the DTBM-SEGPHOS system, no induction period was observed. As such, we were able to rigorously determine the effect of substrate, product, and catalyst concentration on the rate of catalysis using initial rates. The rate has an inverse dependence on the substrate concentration as illustrated in Figure 8. Rate eq 14 was derived for the initial rate of reaction in which $K_{eq}$ represents the equilibrium constant between complex **15** and **16** and $k_{cat}$ represents the first order rate constant for conversion of **16** to product (see Supporting Information for derivation).

$$\text{rate}_{\text{initial}} = \frac{K_{eq}k_{cat}[\text{cat}]}{[\mathbf{1a}] + K_{eq}} \qquad (14)$$

This initial rate law (assuming negligible decarbonylation and product concentration) is consistent with the apparent equilibrium mixture of **15** and **16** observed by NMR and the relationship observed between rate and [**1a**] as depicted in Figure 8.[36] At higher substrate concentrations, the rate is expected to be slower because resting state **15** would be favored. Next, we

(35) Of note, when the *t*Bu-substituted ketone **1k** was added (20 equiv) to a solution of Rh((*R*)-DTBM-SEGPHOS)]$BF_4$ in $CD_2Cl_2$, the spectrum showed only one doublet ($\delta$ 39.1, $J$ = 201 Hz). We believe the steric bulk of the *t*Bu group prevents coordination of a second equivalent of substrate.

(36) See Supporting Information for a discussion of how $K_{eq}$ can be estimated by two complementary methods.

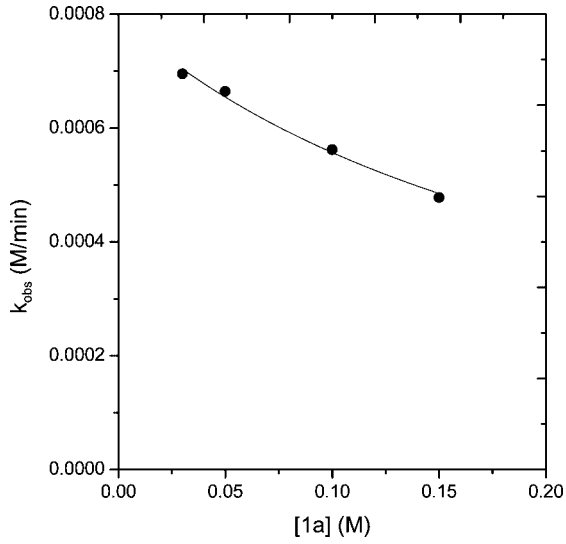


***Figure 8.*** Plot of $k_{obs}$ vs [**1a**] with [Rh((*R*)-DTBM-SEGPHOS)]$BF_4$ (0.005M). The curve describes a least-squares fit to $k_{obs} = a/(b + [\mathbf{1a}])$ ($a = 1.9 \times 10^{-4} \pm 0.1 \times 10^{-4}$; $b = 0.24 \pm 0.02$).

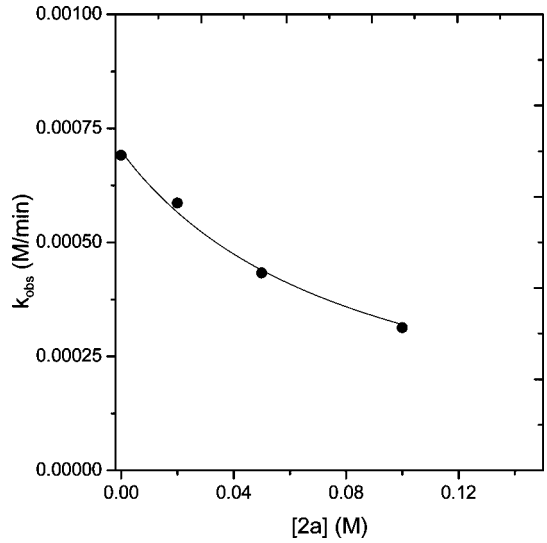


***Figure 9.*** Plot of $k_{obs}$ vs the concentration of product **2a** added at the start of the reaction. The curve describes a linear least-squares fit to $k_{obs} = a/([\mathbf{2a}] + b)$ ($a = 5.9 \times 10^{-5} \pm 0.4 \times 10^{-5}$, $b = 0.084 \pm 0.006$).

constructed a plot of the initial rate of reaction versus the concentration of added product (Figure 9). This plot demonstrates competitive product inhibition[37] and supports the proposed equilibrium between substrate-bound complex **19** and product-bound complex **16** shown in Scheme 4.

The order in catalyst was determined to be first order which is also consistent with a mechanism involving a monomeric catalyst (Figure 10). However, this catalytic process is complicated by a competing substrate decarbonylation side reaction that leads to catalytically inactive rhodium carbonyl species **21** ($^{31}$P NMR: $\delta$ 22.82, $J = 122.8$ Hz). It is possible that CO could dissociate from the catalyst to reform a catalytically active species, but we assume this dissociation is sluggish at room temperature.[16a]

Finally, the mechanistic proposal summarized in Scheme 4 was fit to the experimental data using the kinetics modeling

(37) See Supporting Information for a rate law describing substrate and product dependences.

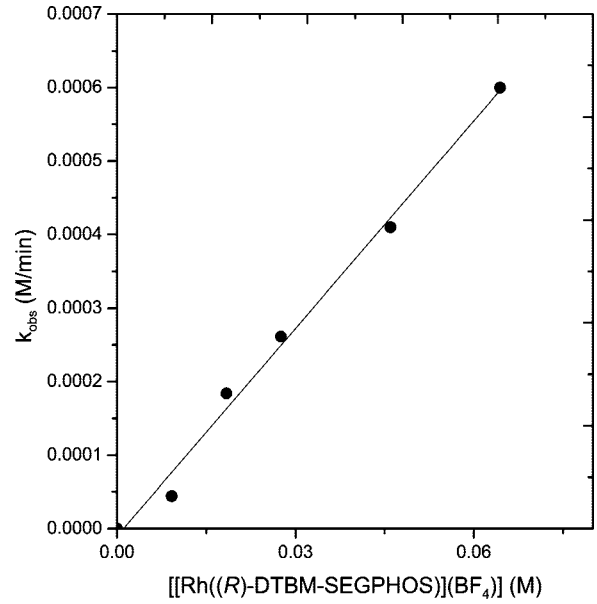


***Figure 10.*** Plot of $k_{obs}$ vs [Rh((*R*)-DTBM-SEGPHOS)]$BF_4$ catalyst concentration. The curve describes a linear least-squares fit to $k_{obs} = m$ [[Rh((*R*)-DTBM-SEGPHOS)]$BF_4$] ($m = 0.0919 \pm 0.0024$).

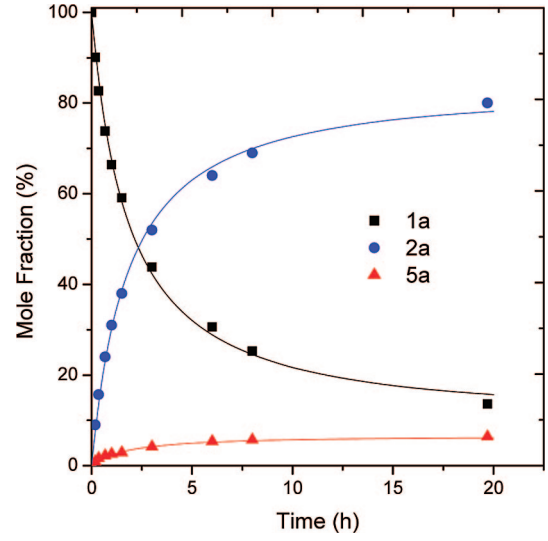


***Figure 11.*** Experimental (data points) and simulated (solid lines) time courses for the formation of **2a** and **5a** with [Rh((*R*)-DTBM-SEGPHOS)]$BF_4$.

software package Copasi[31] (Figure 11). The close fit between the modeled and experimental rates indicate that our proposed mechanism is consistent with the kinetic data.

**Chelation Effect.** As thioethers are well-known to be ligands in chelation assisted hydroacylation, we also investigated thio-based substrates.[18a,38] Substrate **1s** was allowed to react in the presence of $[Rh(dppp)]_2(BF_4)_2$ and [Rh((*R*)-DTBM-SEGPHOS)]-$BF_4$ (eqs 15 and 16). The thiol ether substrate was converted efficiently into chiral lactone **2s** with both ligands. Excellent

(38) (a) Willis, M. C.; McNally, S. J.; Beswick, P. J. *Angew. Chem., Int. Ed.* **2004**, *43*, 340. (b) Willis, M. C.; Randell-Sly, H. E.; Woodward, R. L.; Currie, G. S. *Org. Lett.* **2005**, *7*, 2249. (c) Willis, M. C.; Randell-Sly, H. E.; Woodward, R. L.; McNally, S. J.; Currie, G. S. *J. Org. Chem.* **2006**, *71*, 5291. (d) Bendorf, H. D.; Colella, C. M.; Dixon, E. C.; Marchetti, M.; Matukonis, A. N.; Musselman, J. D.; Tiley, T. A. *Tetrahedron Lett.* **2002**, *43*, 7031.

***Scheme 5.*** Loss of Reactivity with the Removal of the Chelating Ether

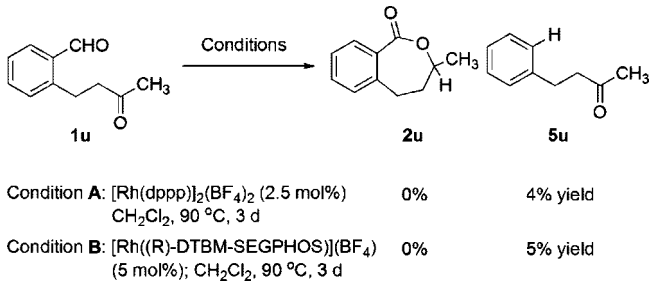


| | | |
|---|---|---|
| Condition **A**: [Rh(dppp)]$_2$(BF$_4$)$_2$ (2.5 mol%) $CH_2Cl_2$, 90 °C, 3 d | 0% | 4% yield |
| Condition **B**: [Rh((*R*)-DTBM-SEGPHOS)](BF$_4$) (5 mol%); $CH_2Cl_2$, 90 °C, 3 d | 0% | 5% yield |

enantioselectivity (>99% ee) was observed in the case with (*R*)-DTBM-SEGPHOS. No decarbonylation was observed with use of either ligand.

However, we found that the keto-aldehyde derivative **1u** bearing a methylene unit in place of a chelating oxygen or sulfur atom shows no desired reactivity with [Rh(dppp)]$_2$(BF$_4$)$_2$ or [Rh((*R*)-DTBM-SEGPHOS)]BF$_4$ (Scheme 5). These results support our hypothesis that a heteroatom plays a crucial role in the catalytic cycle by coordinating to the rhodium center. The precise role of the chelating atom during catalysis cannot be determined easily by experiment because this understanding requires structural knowledge of inobservable intermediates. To understand more elusive details of this mechanism, we rely on molecular modeling (see Computational Study).

**Rhodium Hydride Intermediates.** To our surprise, the dichloro-substituted substrate **1t**[39] did not undergo hydroacylation with either [Rh(dppp)]$_2$(BF$_4$)$_2$ or [Rh((*R*)-DTBM-SEGPHOS)]BF$_4$, even at elevated temperatures (eq 17). Presumably, the chloro substituents cause significant steric and electronic perturbations that prevent hydroacylation. To investigate this lack of reactivity, we treated **1t** with stoichiometric [Rh((*R*)-DTBM-SEGPHOS-]BF$_4$ in $CD_2Cl_2$ and monitored the resulting transformation. By $^1$H NMR, we observed a pair of high field signals with coupling constants characteristic of rhodium hydrides (Figure 12). These two resonances appeared as doublet of triplets: one at −15.17 ppm, ($J$(Rh, H) = 22.8 Hz, $J$(P, H) = 13.6 Hz) and the other at −15.63 ppm, ($J$(Rh, H) = 23.6 Hz, $J$(P, H) = 15.2 Hz). Notably, the P−H couplings observed are completely consistent with literature data for rhodium hydrides oriented cis to phosphine ligands.[40] Hence, there are two isomeric octahedral Rh complexes present, each featuring a hydride cis to both phosphorus atoms in the ligand. Due to their geometry, we believe these observable configurational isomers cannot adopt a conformation to allow carbonyl insertion into the Rh−H via a four-membered transition state. (See Computational Study for further discussion on possible coordination geometries for insertion (Figure 15)). Since it is also possible that isomerization to a more reactive geometry could precede insertion, an alternative explanation is that the chlorine substituents prevent insertion for steric reasons. Although hydroacylation was not observed, this experiment provides support for the possibility of C−H bond activation and the intermediacy of a Rh−H species.

**Computational Study.** Bosnich referred to the mechanism of the hydroacylation of 4-pentenals as "a black box" because intermediates in the catalytic cycle could not be observed but only inferred from indirect experiments.[16a] The lack of any spectroscopic evidence for catalytic intermediates of successful hydroacylation in the present study led us to pursue the use of computational techniques. Specifically, the structures in the catalytic cycle were elucidated with density functional theory using a model system and certain features were then explored using the full experimental system.

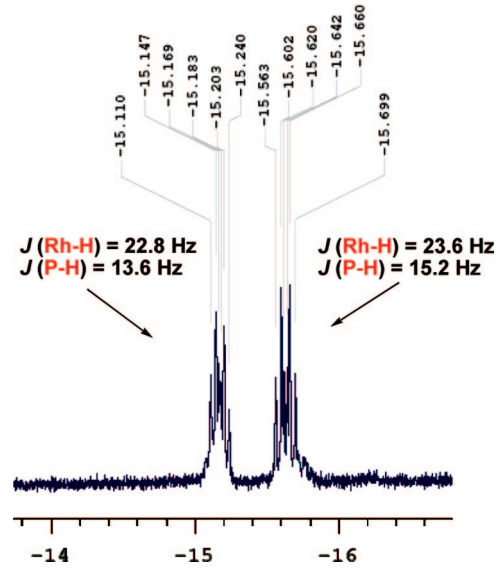


***Figure 12.*** $^1$H NMR spectrum of stable rhodium hydride intermediates **22** formed with substrate **1t** and [Rh((*R*)-DTBM-SEGPHOS)]BF$_4$.

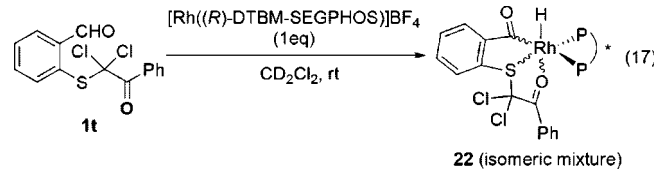


Our calculations on the catalytic cycle were performed using the computational package Jaguar 6.0.[41] To improve computational efficiency, a relatively small ligand, 1,2-bis(dimethylphosphino)benzene was modeled. This ligand was chosen because of its structural and electronic similarity to Me-Duphos. We have shown previously that (*R*,*R*)-Me-Duphos provides excellent reactivity (95% yield), chemoselectivity (<5% decarbonylation), and enantioselectivity (82% ee) in the ketone hydroacylation of **1a**.[14] We chose Becke's three-parameter hybrid functional B3LYP,[42] as it has been successfully used in other DFT studies featuring Rh(I)/Rh(III) catalytic cycles (including rhodium catalyzed decarbonylation,[43] C−H activation of N-heterocycles,[44] [5 + 2]-cycloadditions,[45] [2 + 2 + 1]-carbocyclizations[46] and asymmetric hydrogenation[47]). The triple-ζ LACV3P** basis set was chosen, which uses the

(39) Substrate **1t** was inadvertantly synthesized via a Swern oxidation of the keto-alcohol precursor of **1s**. See Supporting Information for details.
(40) (a) Carlton, L.; Fernandes, M. A.; Sitabule, E. *Proc. Natl. Acad. Sci. U.S.A.* **2007**, *104*, 6969. (b) Okazaki, M.; Ohshitanai, S.; Tobita, H.; Ogino, H. *Chem. Lett.* **2001**, 952.
(41) *Jaguar 6.0*; Shrodinger, LLC: New York, 2005.
(42) (a) Becke, A. D. *J. Chem. Phys.* **1993**, *98*, 5648. (b) Lee, C. T.; Yang, W. T.; Parr, R. G. *Phys. Rev. B* **1988**, *37*, 785.
(43) Fristrup, P.; Kreis, M.; Palmelund, A.; Norrby, P.-O.; Madsen, R. *J. Am. Chem. Soc.* **2008**, *130*, 5206.
(44) Wiedemann, S. H.; Lewis, J. C.; Ellman, J. A.; Bergman, R. G. *J. Am. Chem. Soc.* **2006**, *128*, 2452.
(45) Yu, Z. X.; Cheong, P. H. Y.; Liu, P.; Legault, C. Y.; Wender, P. A.; Houk, K. N. *J. Am. Chem. Soc.* **2008**, *130*, 2378.
(46) Pitcock, W. H., Jr.; Lord, R. L.; Baik, M.-H. *J. Am. Chem. Soc.* **2008**, *130*, 5821.
(47) Gridnev, I. D.; Imamoto, T.; Hoge, G.; Kouchi, M.; Takahashi, H. *J. Am. Chem. Soc.* **2008**, *130*, 2560.

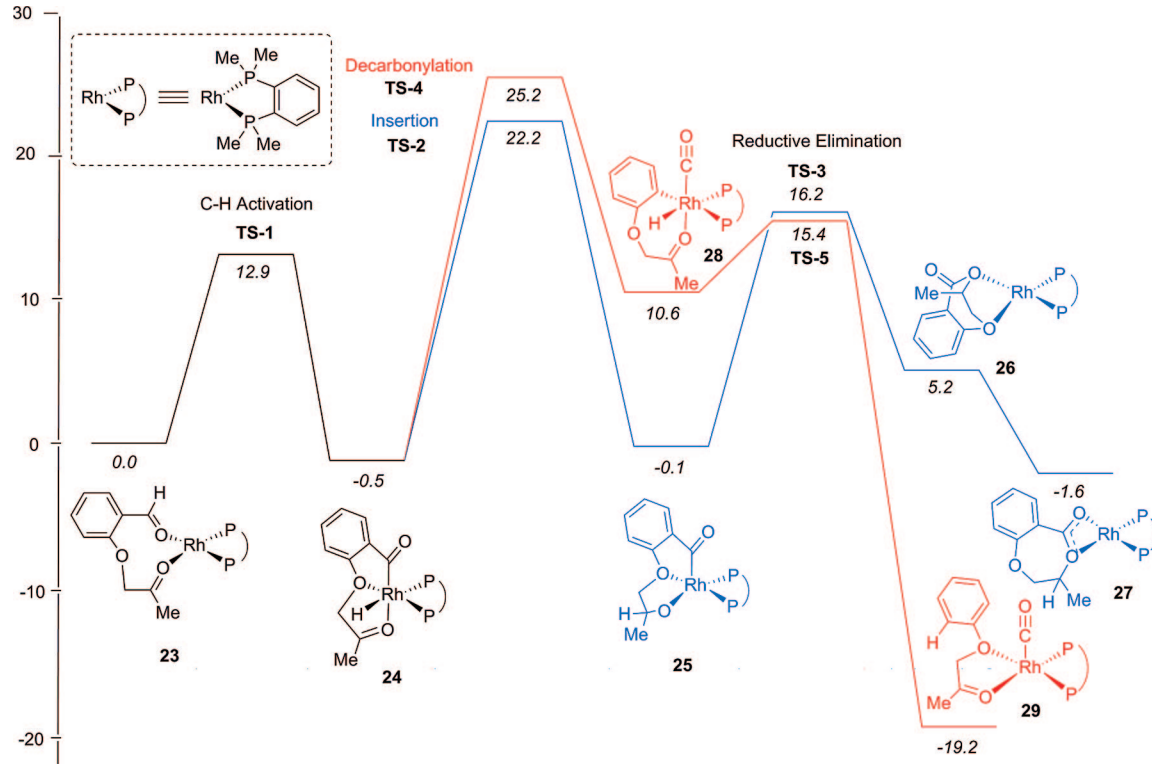


***Figure 13.*** Free energy profile (298 K, 1 atm) for ketone hydroacylation calculated at the B3LYP LACV3P** level, (see Supporting Information for details).

6-311G** basis set for H, C, O, and P atoms and features effective core potentials developed by Hay and Wadt[48] for Rh. Analytical frequency calculations were performed to confirm the nature of all optimized structures and to determine free energies using standard gas phase corrections.[49]

Our calculations have shown that initial binding of the substrate to the catalyst to give **23** occurs with coordination of the ketone and aldehyde oxygen to form a square planar Rh(I) complex (Figure 13). However this coordination geometry is only 1.3 and 1.5 kcal/mol lower in energy than geometries where the aldehyde and ether or the ketone and ether, respectively, are coordinated to rhodium in a square planar complex. It is likely that these modes of coordination can readily exchange. C−H bond activation, however, occurs through a pseudo-octahedral transition state where the ketone and ether oxygen are both coordinated to the rhodium center. None of the possible transition states could be optimized without both of these groups coordinated. The activation barrier to the oxidative addition event is 12.9 kcal/mol (**TS-1**). Chelation of the ether and ketone (see Figure 14) increases the electron density on the rhodium center and, thus, facilitates oxidative addition.

Intermediate **24** is octahedral, with the ketone coordinating to the metal through a lone pair on O, and cis to the hydride. In this geometry, the hydride is coplanar with the two P atoms and the substrate (the acyl, ether and ketone ligands) are themselves coplanar. Three other possible coordination geometries were investigated, where the hydride is oriented cis to both P atoms on the ligand. The hydride could be oriented trans to the acyl-substituent, the ether oxygen, or the ketone ligand. However, the three resulting isomers **30**, **31**, and **32** (Figure 15) would not be able to adopt a conformation that could undergo insertion. Moreover, the energies of these isomeric complexes **30**, **31**, and **32** were determined to be 16.8, 7.0, and 2.9 kcal/mol less stable than **24**, respectively.

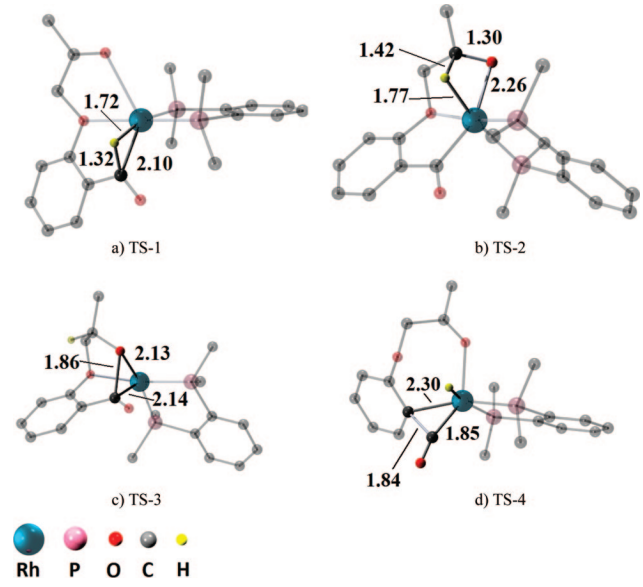


***Figure 14.*** Optimized transition state structures: (a) C−H activation; (b) ketone insertion; (c) reductive elimination; (d) decarbonylation. Relevant interatomic distances are shown in Å.

The transition state for insertion of a rhodium hydride into a carbon−carbon double bond (during olefin hydroacylation) is a planar four-membered structure because the $\pi$-bond interacts with a d orbital on rhodium. In the case of a carbonyl double bond (during ketone hydroacylation, **TS-2**), there exist possible interactions between Rh and the lone pairs on the ketone oxygen.

(48) Hay, P. J.; Wadt, W. R. *J. Chem. Phys.* **1985**, *82*, 299.
(49) Cramer, C. J., *Essentials of Computational Chemistry*, 2nd ed.; John Wiley and Sons: New York, 2004.

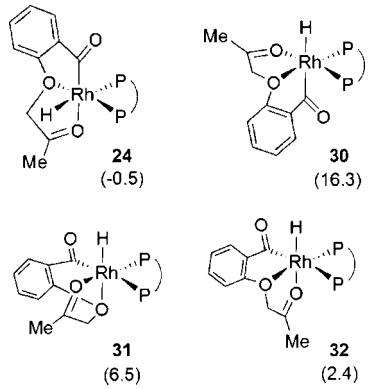


***Figure 15.*** Alternative coordination geometries for the intermediate after C−H bond activation (free energy in kcal/mol relative to **23**).

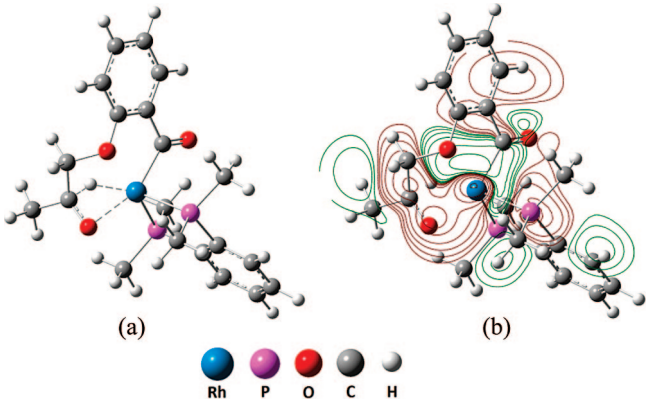


***Figure 16.*** HOMO of the ketone insertion transition state: (a) geometry of the transition state; (b) contour plot of the HOMO in the plane defined by Rh, C (ketone), and O (ketone) displaced by 0.5 Å along the normal vector away from the hydride. The red lobes surrounding the ketone involve an interaction between a lone pair on oxygen and a $d_{z^2}$ orbital on Rh.

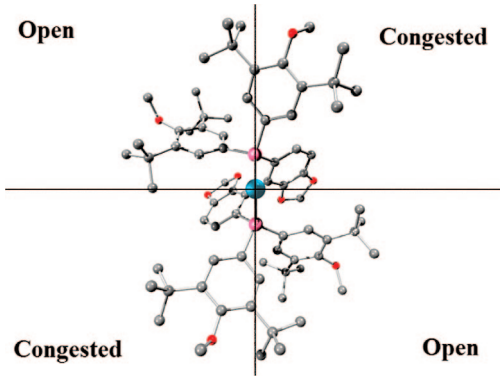


***Figure 17.*** Minimized structure of [Rh((*R*)-DTBM-SEGPHOS)]$^+$; top right and bottom left quadrants are sterically crowded due to the bulky aryl groups, while the aryl groups in the top left and bottom right quadrants points away from the viewer.

Of note, the transition state geometry for **TS-2** is distorted by 26° from planarity (Figure 14b). We believe this distortion results from the strain of the [2.1.1]-bicyclic transition state due to the coordination of the ether oxygen. It is possible that this distortion from planarity is compensated to some degree by overlap of the O lone pair and a Rh d orbital. Indeed, the HOMO for the transition state shows significant overlap between the O lone pair and the Rh $d_{z^2}$ orbital (Figure 16). This is corroborated by the calculated Mayer bond order[50] of 0.45 between the ketone O and Rh.

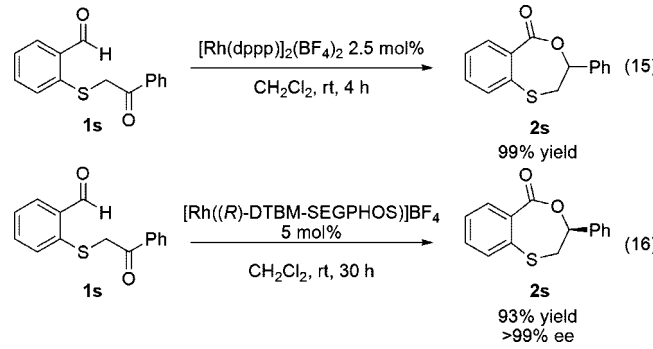


Insertion results in formation of intermediate **25**, which is square pyramidal with the acyl group at the apical position. The preference for an apical acyl group in square-pyramidal intermediates during hydroacylation has previously been noted by Sargent[16e] and by Wu,[51] and this preference was attributed to the high trans effect of the acyl ligand. Reductive elimination of the alkoxide and acyl ligands occurs with an activation barrier of 16.2 kcal/mol and proceeds through a three-center transition state (**TS-3**), with the Rh−C and Rh−O bonds at 2.13 and 2.14 Å, respectively, as shown in Figure 14c. The product resulting from reductive elimination is initially coordinated to the catalyst through the ether and lactone (ether) oxygen atoms in a square planar geometry (**26**). Structure **27** possesses a more favorable binding mode of the product to the catalyst. In this structure, the product is bound by both oxygen atoms of the lactone. The regeneration of **23** from **27** by displacement of the product with the substrate is calculated to be downhill by 5.1 kcal/mol.

According to these calculations, ketone insertion has the highest energy transition state of the three elementary steps involved in hydroacylation, and hence, this step is predicted to be rate-limiting. Notably, this prediction is consistent with our experimental data. The calculated kinetic isotope effect of 1.3 is in reasonable agreement with the experimentally determined kinetic isotope effect of 1.79 for dppp. It should be noted that these results are not directly comparable since they involve different ligands.

Decarbonylation is a competitive side reaction that can occur following C−H activation. The calculated barrier for decarbonylation is 3.0 kcal/mol higher than for ketone insertion. This small difference in energy barriers is consistent with the large dependence of the product ratio on the ligand. For example, in the MeO-BIPHEP series (Table 4) variation of the aryl group had a significant effect on the extent of decarbonylation. With ligand **L1** (R = Ph), 98% of the decarbonylated product was observed at 120 °C. However with **L4** (R = 3,5-*t*Bu-4-MeO-Ph), only 31% decarbonylation product was observed, with 63% desired lactone obtained. Furthermore, no decarbonylation was observed within the limits of experimental detection for dppp. Since changes in ligand structure and electronic properties can have such a large influence on the course of the reaction, it is not surprising that the calculated barriers for insertion and decarbonylation are so similar. Following reductive elimination of the decarbonylated arene product, the rhodium carbonyl species **29** is formed. This is predicted to be 19.2 kcal/mol lower in energy than the substrate-catalyst complex **23**.

**Origin of Enantioselectivity.** In order to explain the sense of enantioinduction observed using the (*R*)-DTBM-SEGPHOS

(50) Mayer, I. *Chem. Phys. Lett.* **1983**, *97*, 270.
(51) Chung, L. W.; Wu, Y. D. *J. Theoret. Comp. Chem.* **2005**, *4*, 737.

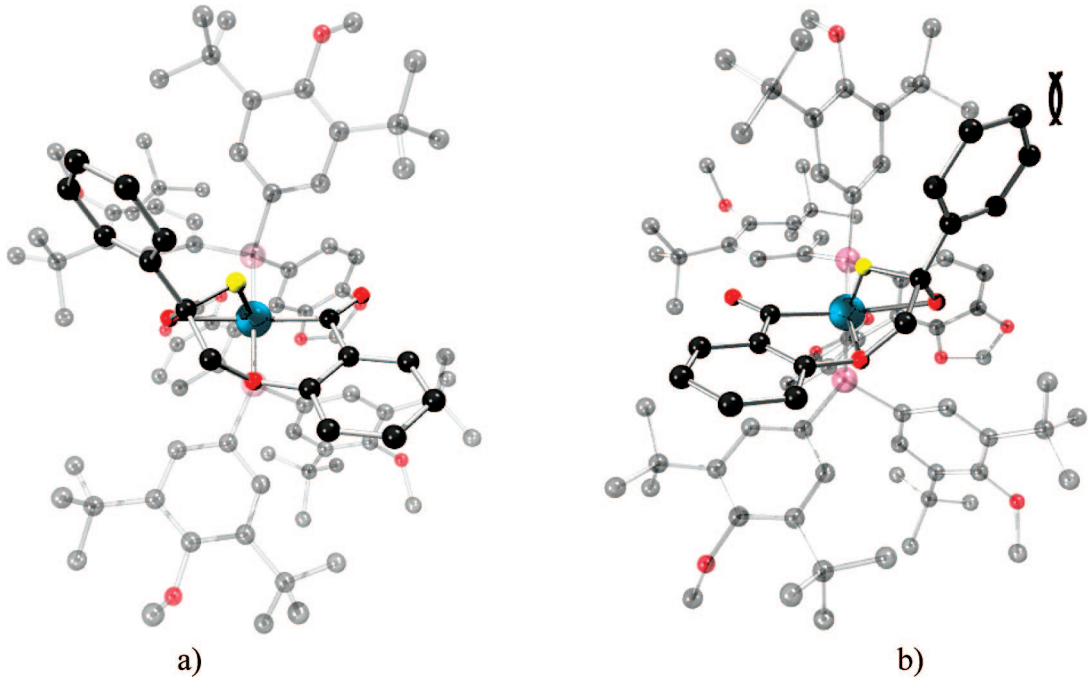


***Figure 18.*** (a) Minimized transition-state analogue leading to the observed major enantiomer with C−H bond constrained to the distance found for **TS-2**. (b) Minimized transition-state analogue leading to the minor enantiomer with C−H bond constrained to the distance found for **TS-2**. Steric interactions with the bulky aryl group cause unfavorable structural reorganization as the aryl group must rotate to accommodate the phenyl group of the substrate.

ligand, a series of constrained geometry optimizations of the full catalyst [Rh((*R*)-DTBM-SEGPHOS)]$^+$ was performed with DFT at the B3LYP/Lanl2DZ[48] level with the Gaussian '03 package.[52] Due to the large size of this system (over 200 atoms) a smaller double-$\zeta$ basis set was used for these calculations as compared to the triple-$\zeta$ basis set used to study the full catalytic cycle of the model system.

The catalyst, as shown in Figure 17, is $C_2$ symmetric. When looking down a Rh−P bond with the ligand pointing away from the viewer, the field of view can be divided into four quadrants. The top right and bottom left quadrants are sterically congested due to the bulky 3,5-*t*Bu-4-MeO-Ph- group. However, the bottom right and top left quadrants are open as the bulky aryl group is pointing away from the viewer. From the model system, ketone insertion is predicted to be the enantiodiscriminating and rate-limiting step of the catalytic cycle, which also suggests that the C−H bond activation is reversible. In contrast, Bosnich found that for the kinetic resolution of chiral 4-pentenals, there was no single enantiodiscriminating step but rather many steps that contributed to the enantioselectivity.[16b] An approximate transition state for [Rh((*R*)-DTBM-SEGPHOS)]$^+$ (with the phenyl-ketone substrate **1a** undergoing ketone insertion) was calculated by constraining the hydride-ketone C−H bond length to 1.42 Å (the bond length calculated for the transition state in the model system, **TS-2**). While this is not a true transition-state optimization, we believe that the geometry of the transition state in the model system should be similar, and therefore, the constrained optimization should provide a clear rationale for the observed sense of induction. Shown in Figure 18a, the phenyl group is projected into an empty quadrant. From this transition state geometry the resulting product is predicted to have the *S* absolute configuration. Importantly, the model predicts the absolute configuration that is consistent with our experimental observations as determined by single-crystal X-ray analysis.[14] The corresponding diastereomeric transition state (Figure 18b) would place the phenyl group in one of the sterically congested quadrants and significant, unfavorable structural reorganization would have to occur to accommodate this configuration. The calculated energy difference between the diastereomeric transition states is 4.9 kcal/mol.

## Conclusion

Experimental and theoretical studies were undertaken in order to understand the mechanism of the recently reported Rh(I)-catalyzed intramolecular ketone hydroacylation.[14] KIE and Hammett plot studies indicated that insertion of the ketone into the rhodium hydride is the rate-limiting step, a proposal consistent with the calculated reaction barriers. Kinetic studies indicated that when dppp is used as the ligand, a stable catalyst dimer slowly dissociates, mediated by the substrate, into catalytically active monomeric catalyst−substrate complexes. Following the reductive elimination step of the catalytic cycle, the product is bound to the catalyst, and this species accumulates over the course of the reaction. Replacement of the product with the substrate leads to catalytic turnover. With (*R*)-DTBM-SEGPHOS, steric bulk precludes the formation of a dimeric catalyst structure, and therefore, the resting state is monomeric

(52) Frisch, M. J.; Trucks, G. W.; Schlegel, G. E.; Scuseria, M. A.; Robb, M. A.; Cheeseman, J. R.; Montgomery Jr., J. A.; Vreven, T.; Kudin, K. N.; Burant, J. C.; Millam, J. M.; Iyengar, S. S.; Tomasi, J.; Barone, V.; Mennucci, B.; Cossi, M.; Scalmani, G.; Rega, N.; Petersson, G. A.; Nakatsuji, H.; Hada, M.; Ehara, M.; Toyota, K.; Fukuda, R.; Hasegawa, J.; Ishida, M.; Nakajima, T.; Honda, Y., Kitao, O.; Nakai, H.; Klene, M.; Li, X.; Knox, J. E.; Hratchian, H. P.; Cross, J. B.; Adamo, C.; Jaramillo, J.; Gomperts, R.; Stratmann, R. E.; Yazyev, O.; Austin, A. J.; Cammi, R.; Pomelli, C.; Ochterski, J. W.; Ayala, P. Y.; Morokuma, K.; Voth, G. A.; Salvador, P.; Dannenberg, J. J.; Zakrzewski, V. G.; Dapprich, S.; Daniels, A. D.; Strain, M. C.; Farkas, O.; Malick, D. K.; Rabuck, A. D.; Raghavachari, K.; Foresman, J. B.; Ortiz, J. V.; Cui, Q.; Baboul, A. G.; Clifford, S.; Cioslowski, J.; Stefanov, B. B.; Liu, G.; Liashenko, A.; Piskorz, P.; Komaromi, I.; Martin, R. L.; Fox, D. J.; Keith, T.; Al-Laham, M. A.; Peng, C. Y.; Nanayakkara, A.; Challacombe, M.; Gill, P. M. W.; Johnson, B.; Chen, W.; Wong, M. W.; Gonzalez, C.; Pople, J. A. *Gaussian 03, Revision C.02*; Gaussian Inc.: Wallingford CT, 2004.

catalyst bound to one or two substrate molecules, leading to substrate inhibition kinetics. Moreover, competitive decarbonylation removes active catalyst from solution and this catalyst deactivation decreases the observed rate of reaction. A model is proposed to explain the origin of enantioselectivity obtained. We expect that the mechanistic insights gained from this combined experimental and computational study will facilitate the development of new and improved catalysts for ketone hydroacylation.

**Acknowledgment.** Financial support was provided by the University of Toronto, the Canada Foundation for Innovation, Ontario Research Foundation, and NSERC. V.M.D. thanks Boehringer Ingelheim for a Young Investigator Award. P.K.D. and H.A.K. are grateful for an NSERC CGS-M fellowship and Edwin Walter and Margery Warren OGSST fellowship, respectively. Chris Rowley and Mark Taylor are acknowledged for helpful discussions. The Lautens and Batey research groups are thanked for help with chiral HPLC analysis. We appreciate Solvias and Takasago for generous donations of chiral diphospine ligands.

**Supporting Information Available:** Experimental procedures, kinetic data, X-ray crystallographic and spectroscopic data for new compounds, computational details and Cartesian coordinates of all calculated species. This material is available free of charge via the Internet at http://pubs.acs.org.

JA806758M